

CollabOD: Collaborative Multi-Backbone with Cross-scale Vision for UAV Small Object Detection

Xuecheng Bai^{1,*}, Yuxiang Wang^{2,*}, Chuanzhi Xu^{2,†}, Boyu Hu³, Kang Han^{1,4}, Ruijie Pan¹, Xiaowei Niu⁵, Xiaotian Guan⁵, Liqiang Fu⁵, Pengfei Ye⁶

Abstract—Small object detection in unmanned aerial vehicle (UAV) imagery is challenging, mainly due to scale variation, structural detail degradation, and limited computational resources. In high-altitude scenarios, fine-grained features are further weakened during hierarchical downsampling and cross-scale fusion, resulting in unstable localization and reduced robustness. To address this issue, we propose CollabOD, a lightweight collaborative detection framework that explicitly preserves structural details and aligns heterogeneous feature streams before multi-scale fusion. The framework integrates Structural Detail Preservation, Cross-Path Feature Alignment, and Localization-Aware Lightweight Design strategies. From the perspectives of image processing, channel structure, and lightweight design, it optimizes the architecture of conventional UAV perception models. The proposed design enhances representation stability while maintaining efficient inference. A unified detail-aware detection head further improves regression robustness without introducing additional deployment overhead. The code are available at: <https://github.com/Bai-Xuecheng/CollabOD>.

I. INTRODUCTION

Unmanned aerial vehicles (UAVs) have become essential platforms for autonomous perception in applications such as urban traffic monitoring [1], traffic flow analysis [2], and parking management [3]. In these scenarios, object detection plays a critical role in reliable traffic state assessment by accurately identifying and localizing targets in aerial imagery. However, high-altitude operation introduces significant scale variation, a large number of distant small objects, and limited onboard computational resources, making lightweight yet accurate detection models highly desirable.

From a feature representation standpoint, small aerial objects typically smaller than 32×32 pixels contain extremely limited discriminative information. Their features are rapidly degraded through repeated downsampling, leading to weak representations [4] and low signal-to-noise ratios [2], especially under challenging aerial conditions such as low contrast [5], motion blur [6] and atmospheric distortion [4].

*Equal contribution.

†Corresponding authors: Xuecheng Bai (bai_xuecheng@163.com) and Chuanzhi Xu (chuanzhi.xu@sydney.edu.au).

¹Xuecheng Bai, Kang Han and Ruijie Pan are with Aviation Traffic Control Technology (SHENZHEN) Co., Ltd., Shenzhen, China

²Yuxiang Wang and Chuanzhi Xu are with The University of Sydney, NSW, Australia

³Boyu Hu is with The University of International Business and Economics, Beijing, China

⁴Kang Han is with Research Institute of Traffic Control Technology Co., Ltd., Beijing, China

⁵Xiaowei Niu, Xiaotian Guan and Liqiang Fu are with Guoneng Shuohuang Railway Development Co., Ltd., Hebei, China

⁶Pengfei Ye is with The Hong Kong University of Science and Technology, Hong Kong, China

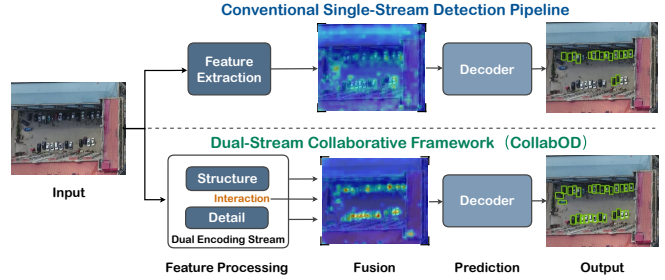


Fig. 1. Comparison of conventional single-stream detection and CollabOD. Single-stream methods attenuate structural cues and perform implicit fusion, resulting in spatial misalignment. CollabOD decouples and aligns structural and detail representations prior to fusion for improving stability and accuracy.

In such cases, fine-grained structural cues, e.g., object boundaries and edge textures, become critical for distinguishing foreground from background, thereby requiring precise localization [3], [7]. Although feature pyramid networks preserve multi-scale representations, their cross-scale fusion is usually implemented via simple addition or concatenation, lacking explicit modeling of structural detail attenuation and cross-layer misalignment.

Existing methods enhance representation capacity by introducing auxiliary branches [3], [8], attention mechanisms [3], or refined fusion strategies [6], [9]. While effective, these designs often produce heterogeneous feature streams with distinct receptive field distributions and semantic biases. Conventional fusion implicitly assumes spatial and semantic compatibility across paths, making it difficult to explicitly suppress cross-path discrepancies. For small objects with inherently limited structural and semantic representations, even minor spatial misalignment can be amplified during bounding box regression, leading to localization instability and degraded robustness. Consequently, UAV small object detection is jointly constrained by structural detail attenuation and implicit cross-path fusion inconsistency.

To address these issues, we explicitly enhance structural detail preservation and calibrate heterogeneous feature streams prior to fusion, as shown in Fig. 1. We believe, firstly, localization-related structural cues should be explicitly enhanced under lightweight constraints. Secondly, heterogeneous feature streams should be calibrated prior to fusion to improve spatial and semantic compatibility.

In this paper, we propose **CollabOD**, a collaborative small object detection framework built upon YOLO11-M-P2 [10]. CollabOD systematically improves input encoding, backbone

representation, multi-scale fusion, and detection head design to achieve structural detail enhancement, cross-path alignment, and computational efficiency. Experiments on VisDrone [11], UAVDT [12] and AI-TOD [13] show that CollabOD improves detection robustness in challenging aerial scenes. It achieves state-of-the-art AP₇₅ on VisDrone [11] while using the lowest GFLOPs, and obtains the best AP₅₀ and AP_{50:95} on UAVDT [12], indicating a strong accuracy–efficiency trade-off. On AI-TOD [13], our model further establishes state-of-the-art performance in AP₅₀, AP_{50:95}, GFLOPs, and FPS, simultaneously achieving the highest detection accuracy and the most favorable computational efficiency.

The main contributions of this work are summarized as follows:

- We develop a lightweight detection framework **CollabOD** that jointly enhances structural details and aligns heterogeneous feature streams, ensuring stable localization and high detection accuracy for small objects under limited computational budgets.
- We design a **Dual-Path Fusion Stem (DPF-Stem)** and a **Dense Aggregation Block (DABlock)** to mitigate the progressive degradation of localization-related structural information in deep networks, preserving boundary and contour cues at the input stage while compensating for hierarchical feature attenuation.
- We introduce a **Bilateral Reweighting Module (BRM)** that improves cross-scale feature consistency through channel-wise adaptive weight generation and learnable scaling.
- We propose a **Unified Detail-Aware Head (UDA Head)** that enhances boundary regression via detail-aware convolution and employs re-parameterization to eliminate additional inference overhead.

II. RELATED WORK

This section reviews recent advances in UAV small object detection, focusing on structural representation, cross-scale feature learning, and efficiency-aware localization design from the perspective of localization stability under deployment constraints.

A. Structural Representation for Small Objects

For small object detection in UAV aerial imagery, structural representation capability can be characterized along two dimensions: the supply strength of structural information for small objects, and the stability of structural features during hierarchical propagation. Related research has primarily evolved along two corresponding paths: detail supply and structural compensation.

At the information supply level, early methods typically increase effective pixels through higher input resolution [14], slice / patch-based inference [15], or super-resolution assistance [16], yet offer limited mitigation of structural information degradation caused by deep downsampling. More recent detection frameworks explicitly introduce higher-resolution feature layers [1] or adjust pyramid allocation strategies [17]

to preserve fine-grained structures, thereby enhancing the initial representational capacity of structural information.

At the propagation stability level, advanced techniques focus on edge-sensitive enhancement [18], local context modeling [19], and multi-path representation design [20] to strengthen the cross-layer transmission of structural cues, shifting small object representation from single-path enhancement toward multi-source collaborative expression. The prevailing trend suggests that jointly improving structural information supply and propagation stability within a unified framework can more robustly support fine-grained localization of small objects in aerial imagery.

However, under lightweight deployment constraints in UAV systems, how to explicitly enhance localization-related structural information remains a key issue.

B. Cross-Scale and Multi-Branch Feature Learning

The core objective of cross-scale and multi-branch designs lies in enhancing feature interaction to improve the representational stability of small objects in complex scenes. Early methods, represented by FPN [21], achieve progressive fusion of multi-scale features through hierarchical pyramid structures; PANet [22] or PAFPN [23] further strengthen bidirectional information flow, while NAS-FPN [8] and ASF [24] improve cross-scale integration flexibility through adaptive redistribution and structural optimization.

With the evolution of network architectures, multi-branch detection frameworks and multi-backbone designs [25] introduce parallel representation pathways that enhance feature diversity and complementary expression through differentiated structures and explicit interaction mechanisms; MoE [26], cross-branch gating [27], and collaborative distillation models [28] further model inter-path information selection and synergy, transitioning feature fusion from implicit aggregation toward explicit interaction and dynamic collaboration.

Despite the continuous evolution of cross-scale feature interaction mechanisms, existing methods still provide limited modeling of consistency between heterogeneous feature streams prior to fusion, which in UAV scenarios may amplify spatial and semantic misalignment and thus impair fine-grained localization stability.

C. Localization and Efficient Detection Design

Feature representation and interaction mechanisms must ultimately translate into stable localization and efficient inference. To improve regression quality, modern detectors adopt decoupled classification and regression branches [29] and integrate IoU-based losses such as GIoU [30], EIoU [31], and DIoU [32] to enhance bounding box stability. Given the sensitivity of small objects to fine-grained structural cues, several approaches further refine regression design or strengthen boundary-aware representations. Structural reparameterization and lightweight backbones are further employed to balance efficiency and representational capacity, enabling deployment in computationally constrained environments.

Taken together, a collaborative mechanism across representation, interaction, and prediction becomes increasingly important for robust deployment.

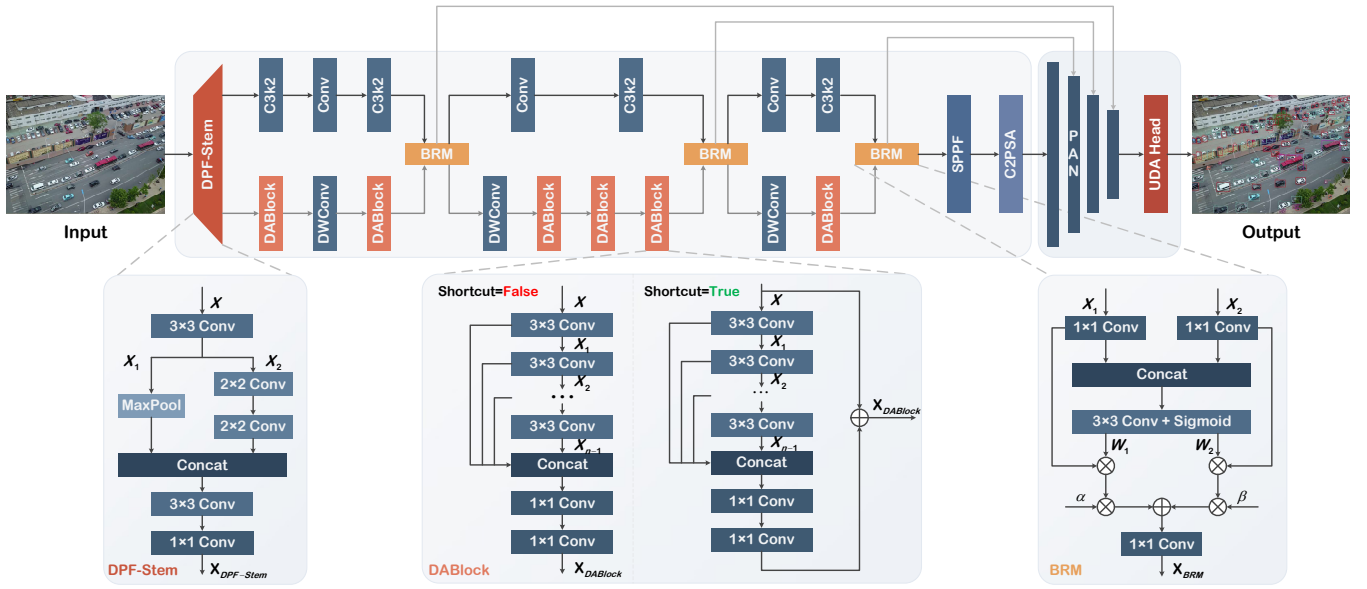


Fig. 2. Overview of the proposed CollabOD framework. DPF-Stem denotes the Dual-Path Fusion Stem, DABlock represents Dense Aggregation Block, and BRM refers to Bilateral Reweighting Module. The UDA Head corresponds to the Unified Detail-Aware Head, which is detailed in Section III-C. The remaining components are inherited from the original YOLO11 architecture.

III. METHODOLOGY

In this section, we present CollabOD, a lightweight small object detection framework for UAV imagery, as shown in Fig. 2. Considering the instability introduced by structural degradation and cross-path inconsistency under lightweight deployment constraints, we focus on two aspects: enhancing localization-related structural information and improving the consistency of heterogeneous feature streams prior to fusion. Accordingly, the proposed framework consists of three collaborative components: Structural Detail Preservation, Cross-Path Feature Alignment, and Localization-Aware Lightweight Design. The three proposed mechanisms are discussed in detail in Sections III-A, III-B, and III-C, respectively.

A. Structural Detail Preservation

Small object cues critical for precise localization in UAV imagery mainly reside in boundary contours and texture gradients. However, repeated downsampling in deep backbones progressively attenuates such high-frequency responses. To mitigate structural decay at both the input and backbone stages, we design a **Dual-Path Fusion Stem (DPF-Stem)** for early preservation and a **Dense Aggregation Block (DABlock)** for hierarchical compensation.

a) Dual-Path Fusion Stem: Given the input feature $X \in \mathbb{R}^{C \times H \times W}$, the core principle of the DPF-Stem is to partition the features into two complementary streams: a structure stream and a detail stream. First, the input feature is embedded and split:

$$\{X_s, X_d\} = \text{Split}(\phi(X)), \quad (1)$$

where $\phi(\cdot)$ denotes a lightweight feature embedding, and $\text{Split}(\cdot)$ represents a channel-wise splitting operator. These

two streams are respectively responsible for preserving low-frequency geometric contours and high-frequency texture gradients:

$$Z_s = \Psi_{\text{pool}}(X_s), \quad Z_d = \Psi_{\text{conv}}(X_d), \quad (2)$$

where Ψ_{pool} employs max projection or pooling to aggregate stable structural responses, and Ψ_{conv} is a learnable lightweight convolution designed to preserve texture gradients and local differential responses. Subsequently, the two streams are fused at the same scale to obtain the stem output, following downsampling:

$$X_{\text{DPF}} = \phi_{\text{fuse}}(Z_s \oplus Z_d), \quad (3)$$

where \oplus denotes concatenation, and ϕ_{fuse} is a lightweight projection used for channel mixing and scale alignment. This dual-stream modeling ensures that the DPF-Stem preserves high-frequency structural responses before and after downsampling, thereby mitigating the loss of early structural information.

b) Dense Aggregation Block: Even though structural details are preserved at the input stage, they still suffer from gradual attenuation during repeated downsampling and cross-layer propagation within deep networks. The objective of the DABlock is to compensate for this hierarchical structural attenuation within the backbone by continuously injecting shallow, fine-grained structural responses into deeper features via dense aggregation. Let $\{X_i\}_{i=1}^n$ denote feature maps from preceding stages aligned to the current scale. The DABlock aggregates these features and refines them via stacked convolutions:

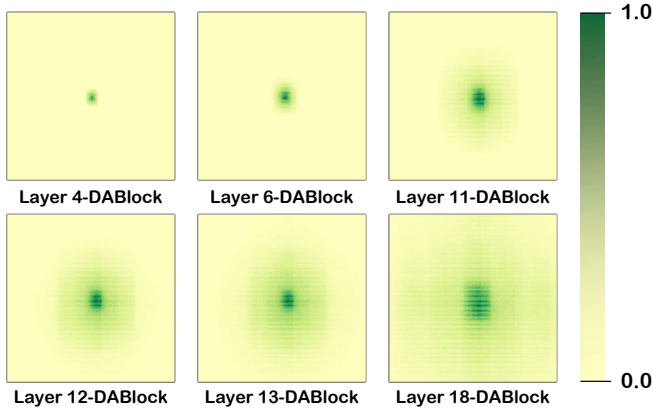


Fig. 3. Effective Receptive Field Visualization Across DABlock Layers.

$$X_{\text{DABlock}} = \psi_{\text{conv}}^{(2)} \left(\bigoplus_{i=1}^n X_i \right) + \delta X, \quad \delta \in \{0, 1\}. \quad (4)$$

Here, \bigoplus denotes feature aggregation, and X is the current-stage input. The residual switch δ preserves identity propagation when enabled. This design effectively reinforces shallow structural cues in deeper representations, thereby mitigating the aforementioned detail attenuation.

From an **Effective Receptive Field** (ERF) perspective, dense aggregation promotes progressive spatial interaction across layers. By integrating aligned multi-level features, DABlock enhances long-range dependency modeling while preserving structural details. As shown in Fig. 3, the ERF expands steadily with depth, exhibiting increasingly broader high-contribution regions.

B. Cross-Path Feature Alignment

To mitigate the inconsistency between heterogeneous feature streams prior to fusion, we construct the **Bilateral Reweighting Module (BRM)** to calibrate the two-stream features prior to the fusion of multiple backbone pathways. Specifically, given two-stream features on the same scale $X^{(1)}, X^{(2)} \in \mathbb{R}^{C \times H \times W}$, we first map the features into a unified embedding space using a lightweight projection (e.g. 1×1 convolution) to obtain $\hat{X}^{(1)}$ and $\hat{X}^{(2)}$. Subsequently, we jointly embed them across pathways to capture the joint context:

$$Z = \psi \left(\left[\hat{X}^{(1)}, \hat{X}^{(2)} \right] \right), \quad (5)$$

where $[\cdot, \cdot]$ denotes concatenation along the channel dimension, and ψ is a lightweight spatial interaction operator used to model cross-pathway dependencies. Then, the bilateral gating masks are generated via activation and splitting:

$$\left[G^{(1)}, G^{(2)} \right] = \text{Split}(\sigma(Z)), \quad (6)$$

where σ represents the sigmoid activation function, and $\text{Split}(\cdot)$ evenly divides the channels to obtain the two-stream masks $G^{(k)} \in (0, 1)^{C \times H \times W}$. Unlike channel-only gating,

Algorithm 1 UDA Head: Unified Detail-Aware Head

Input: Multi-scale features $\{F_i\}_{i \in \{xs, s, m, l\}}$, class number N_c , DFL bins R , hidden dimension C_h

Output: Decoded bounding boxes B and classification scores S

```

1: // Shared projection and detail enhancement
2: for  $i \in \{xs, s, m, l\}$  do
3:    $G_i \leftarrow \mathcal{S}(\text{Conv}_{1 \times 1}(F_i))$ 
4:    $P_i \leftarrow \text{Concat}(s_i \mathcal{H}_{\text{box}}(G_i), \mathcal{H}_{\text{cls}}(G_i))$ 
5: end for
6: // Flatten and merge multi-scale predictions
7:  $Q \leftarrow \text{Concat}_{i \in \{xs, s, m, l\}}(\text{Reshape}(P_i))$ 
8: // Distribution Focal Loss decoding
9:  $(B_{\text{raw}}, C_{\text{raw}}) \leftarrow \text{Split}(Q, \{4R, N_c\})$ 
10:  $D \leftarrow \text{DFL}(B_{\text{raw}})$  ▷ convert distributions to distances
11: // Bounding box decoding
12:  $B \leftarrow \text{Dist2BBox}(D)$ 
13:  $S \leftarrow \sigma(C_{\text{raw}})$ 
14: return  $\text{Concat}(B, S)$ 

```

these masks are spatially dependent, enabling finer suppression of cross-pathway redundancy and biased responses under complex backgrounds.

After obtaining the bilateral masks, the BRM reweighs the two streams and achieves statistical scale calibration prior to fusion via learnable channel amplitude modulation:

$$X_{\text{BRM}} = \phi_{\text{out}} \left(\sum_{k=1}^2 \hat{X}^{(k)} \odot G^{(k)} \odot \lambda^{(k)} \right), \quad (7)$$

where \odot denotes the Hadamard product; $\lambda^{(k)} \in \mathbb{R}^{C \times 1 \times 1}$ is a learnable channel scaling factor designed to balance the response amplitudes of the two streams and stabilize the gradient flow; and ϕ_{out} is a 1×1 projection used for channel mixing and output integration. Through bilateral spatial reweighting and channel calibration, the BRM alleviates cross-pathway discrepancies before fusion, thereby improving feature compatibility and stabilizing the subsequent localization regression.

C. Localization-Aware Lightweight Design

Following structural enhancement and cross-path calibration, the remaining critical challenge is to enable the regression head to stably leverage these structural cues without introducing additional computational overhead during the inference phase. To this end, the proposed **Unified Detail-Aware Head (UDA Head)** strikes a robust balance between localization stability and efficiency through shared detail enhancement and decoupled prediction.

a) *Forward Process:* The specific forward process is summarized in Algorithm 1, where multi-scale features are denoted as F_i .

b) *Complexity Analysis:* The primary computational overhead stems from the shared detail enhancement block \mathcal{S} and the prediction heads. Let $N = \sum_i H_i W_i$ denote the

total number of spatial locations across all scales. The time complexity can be formulated as:

$$\mathcal{O}(NC_h^2) + \mathcal{O}(NC_h) + \mathcal{O}(NR). \quad (8)$$

Typically, since $C_h \gg R$, the dominant term is $\mathcal{O}(NC_h^2)$. The space complexity is primarily composed of the intermediate features and the prediction logits:

$$\mathcal{O}(NC_h) + \mathcal{O}(N(4R + N_c)). \quad (9)$$

Because \mathcal{S} and the projections are shared across all scales, the UDA Head enhances detail perception for regression while maintaining low additional parameter counts and inference overhead, making it highly suitable for UAV deployment scenarios with constrained computational resources.

IV. EXPERIMENTS AND RESULTS

A. Experimental Settings

1) *Implementation Details*: CollabOD is built upon the YOLO11-M-P2 architecture. All experiments are conducted on an NVIDIA RTX 5090D GPU. We use the SGD optimizer with an initial learning rate of 0.01 and momentum of 0.937. The input image size is 640×640, the batch size is 8, and training runs for 500 epochs.

2) *Dataset*: We conduct extensive experiments on three widely used UAV object detection benchmarks, namely VisDrone-2019-DET [11], UAVDT [12] and AI-TOD [13]. **VisDrone-2019-DET [11]** is a widely adopted UAV detection benchmark comprising 10,209 images captured across diverse cities, times, and flight altitudes, covering 10 categories (e.g., van, truck, awning-tricycle) with significant scale variation and complex backgrounds. **UAVDT [12]** is a large-scale traffic-oriented UAV benchmark containing 77,819 annotated frames extracted from 100 video sequences, covering four vehicle categories (car, truck, bus, and other vehicle) across urban roads, intersections, and highways, with rich attribute annotations including weather, altitude, occlusion, and illumination conditions. **AI-TOD [13]** is a dedicated remote sensing benchmark tailored for tiny object detection, containing 28,036 images with 700,621 annotated instances. It covers eight object categories, including bridge, ship, vehicle, storage tank, person, swimming pool, wind mill, and airplane.

3) *Metrics*: We adopt the standard COCO evaluation protocol[42], reporting AP_S , AP_M , AP_{50} , AP_{75} , and $AP_{50:95}$ (averaged over IoU from 0.5 to 0.95 with a step of 0.05) to evaluate detection consistency across varying localization strictness.

B. Results on VisDrone Dataset

1) *Comparative Results*: We compare CollabOD with a broad range of state-of-the-art detectors on the VisDrone-2019-DET benchmark. The quantitative results are summarized in Table I.

With 20.9M parameters and 65.5 GFLOPs, CollabOD achieves 52.4 AP_{50} , 30.8 AP_{75} , and 29.9 $AP_{50:95}$. Among all compared methods, CollabOD attains the highest AP_{75} ,

TABLE I

COMPARATIVE RESULTS ON THE **VisDrone-2019-DET** [11] DATASET. RESULTS OF OTHER METHODS ARE TAKEN FROM THEIR ORIGINAL PUBLICATIONS, AND UNREPORTED METRICS ARE REPRODUCED UNDER THE SAME EVALUATION PROTOCOL FOR FAIR COMPARISON. **BOLD** AND UNDERLINE DENOTE THE BEST AND SECOND-BEST RESULTS, RESPECTIVELY.

Model	Params	GFLOPs	$AP_{50} \uparrow$	$AP_{75} \uparrow$	$AP_{50:95} \uparrow$
PP-YOLOE-SOD-L [33]	42.2	120.5	48.5	<u>30.4</u>	29.7
CFPT [34]	56.3	297.6	38.0	23.1	22.6
QueryDet [35]	33.9	212.0	48.1	28.8	28.3
UAV-OD [36]	–	–	47.6	21.6	24.4
UAV-DETR-R18 [37]	<u>20.0</u>	77.0	48.8	29.2	29.8
UAV-DETR-R50 [37]	42.0	170.0	51.1	30.4	31.5
BRSTD-L [38]	6.3	220.2	58.0	19.5	26.1
UAV-MaLO [39]	21.6	73.6	49.9	–	<u>30.1</u>
YOLO11-M	20.1	68.2	43.3	24.7	26.3
YOLO11-M-P2	20.7	91.3	46.4	25.3	27.3
YOLOv12-M [40]	20.2	<u>67.5</u>	33.6	18.1	19.2
YOLOv12-M-P2 [40]	<u>20.0</u>	77.7	36.2	24.2	21.0
YOLO26-M [41]	20.4	67.9	33.2	15.4	18.6
YOLO26-M-P2 [41]	21.1	91.4	34.1	17.6	21.4
CollabOD(Ours)	20.9	65.5	<u>52.4</u>	30.8	29.9

indicating improved localization stability under stricter IoU thresholds. This gain is consistent with explicitly strengthening localization-related structural cues and improving feature consistency prior to multi-scale fusion, while maintaining low computational cost.

Compared with the widely adopted YOLO11-M-P2, CollabOD improves AP_{50} from 46.4 to 52.4 and AP_{75} from 25.3 to 30.8, corresponding to gains of 6.0 and 5.5 percentage points, respectively. Meanwhile, the computational cost is reduced from 91.3 GFLOPs to 65.5 GFLOPs. This result indicates that enhancing localization-related structural information and calibrating heterogeneous feature streams prior to fusion can improve high-quality localization without increasing inference complexity.

In comparison with transformer-based approaches such as UAV-DETR-R50, which requires 170.0 GFLOPs, CollabOD achieves competitive or superior detection performance with substantially lower computational overhead. These results verify that the proposed framework provides strong localization capability while maintaining practical efficiency, which is particularly important for UAV-based deployment scenarios.

These results position CollabOD as an efficient yet accurate solution for UAV-based small object detection.

To further validate its effectiveness, we present qualitative comparisons in Fig. 4. Even in cluttered scenes with densely distributed small objects, CollabOD maintains concentrated activation responses and stable localization, producing fewer missed detections and more precise bounding boxes.

2) *Ablation Studies*: We conduct a stepwise ablation study on the VisDrone-2019-DET dataset to evaluate the individual contribution of each proposed component. Under identical training settings, DPF-Stem, DABlock, BRM, and UDA Head

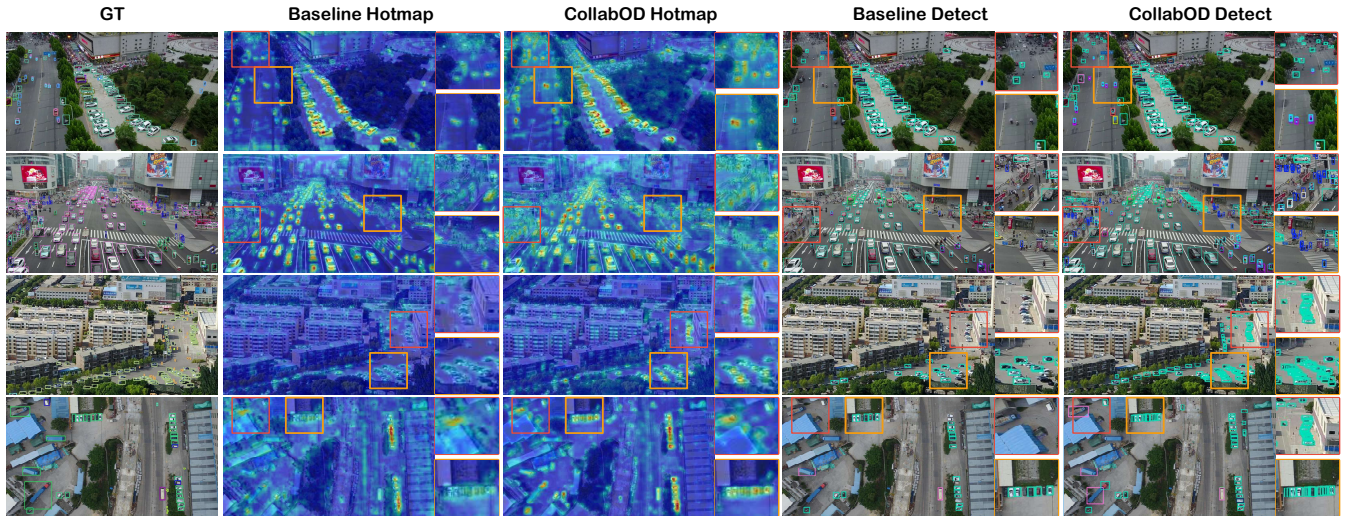


Fig. 4. Qualitative comparison between the baseline and CollabOD on VisDrone-2019-DET. In complex aerial scenes with predominantly small objects, CollabOD exhibits a lower miss rate and more accurate localization than the baseline model.

TABLE II

ABLATION STUDY ON THE **VisDRONE-2019-DET** [11] DATASET. EACH COMPONENT OF THE PROPOSED FRAMEWORK IS INCREMENTALLY ADDED TO EVALUATE ITS INDIVIDUAL CONTRIBUTION. BOLD VALUES INDICATE THE BEST PERFORMANCE.

DPF-Stem	DABlock	BRM	UDA Head	Detection					Complexity	
				AP ₅₀	AP ₇₅	AP _{50:95}	AP _S	AP _M	Params(M)	GFLOPs
				26.2	46.0	25.3	22.7	42.5	27.3	91.3
✓				29.1	39.7	19.9	21.3	41.2	20.9	51.2
✓	✓			40.5	44.6	21.0	24.7	44.5	22.1	68.2
✓	✓	✓		49.1	48.2	27.0	27.2	45.3	29.6	74.8
✓	✓	✓	✓	50.7	52.4	30.8	23.6	47.2	29.9	65.5

are progressively integrated into the baseline detector. The quantitative results are summarized in Table II.

Starting from the baseline, introducing DPF-Stem improves AP₅₀ from 26.2 to 29.1, indicating that enhanced shallow feature modeling benefits small object representation. Although AP₇₅ decreases at this stage, the overall detection performance remains stable while the computational cost is reduced to 51.2 GFLOPs, demonstrating improved efficiency.

After incorporating DABlock, AP₇₅ increases to 44.6, showing improved localization precision under stricter IoU thresholds. In addition, AP_S and AP_M exhibit consistent improvements, validating the effectiveness of adaptive feature enhancement for objects at different scales.

With the introduction of BRM, the detector achieves 49.1 AP₅₀ and 27.0 AP_{50:95}, reflecting improved consistency of heterogeneous feature streams prior to fusion. This module brings a clear improvement in the averaged detection metric across IoU thresholds, indicating enhanced overall detection robustness.

Finally, integrating UDA Head further boosts performance to 50.7 AP₅₀, 52.4 AP₇₅, and 30.8 AP_{50:95}, achieving the best results among all configurations. Compared with the previous variant, AP₇₅ improves by 2.3 percentage points, confirming the effectiveness of the unified detail-aware head

TABLE III

COMPARISON ON THE **UAVDT** [13] DATASET. THE BEST RESULTS AMONG ALL SOTA METHODS ARE HIGHLIGHTED IN **BOLD**.

Model	AP ₅₀ ↑	AP ₇₅ ↑	AP _{50:95} ↑
ClusDet [43]	26.5	12.5	13.7
GLSAN [44]	28.1	18.8	17.0
DREN [45]	–	–	15.1
GFL [46]	29.5	17.9	16.9
CEASC [47]	30.9	17.8	17.1
CollabOD(Ours)	31.2	17.9	17.4

in refining localization quality and stabilizing regression under strict IoU thresholds. Importantly, this accuracy gain is achieved with 65.5 GFLOPs, which remains comparable to the baseline complexity and maintains a favorable trade-off between accuracy and computational cost.

Overall, the consistent improvements across multiple evaluation metrics demonstrate that each component contributes complementary enhancements, leading to a robust and efficient detection framework tailored for UAV-based small object scenarios.

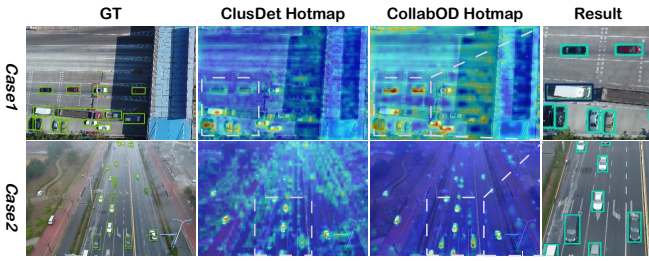


Fig. 5. Visualization of the detection results of ClusDet and the proposed method. Two representative cases are selected, and a focused comparison is conducted on the highlighted regions.

C. Results on UAVDT Dataset

On the UAVDT benchmark, the comparative results are reported in Table III. CollabOD achieves 31.2 AP_{50} , 17.9 AP_{75} , and 17.4 $AP_{50:95}$, obtaining the best AP_{50} and $AP_{50:95}$ among the compared methods. In addition, it ranks second on AP_{75} , indicating stable localization performance under stricter IoU thresholds.

These results demonstrate that the proposed framework generalizes effectively to traffic-oriented UAV scenarios beyond the primary benchmark.

To further examine the model behavior on UAVDT, we provide heatmap visualizations for qualitative analysis. Using the same visualization protocol as in the VisDrone experiments, we compare the activation responses of ClusDet and CollabOD. The visualizations show that CollabOD generates more focused responses around object regions and maintains clearer separation from surrounding background areas, which is consistent with the improved quantitative performance reported in Fig. 5.

D. Results on AI-TOD Dataset

1) *Comparative Results:* On the AI-TOD benchmark, the comparative results are summarized in Table IV. CollabOD achieves 45.4 AP_{50} and 20.0 $AP_{50:95}$, obtaining the best performance among all YOLO-series models on both metrics. Compared with the strongest baseline, it improves AP_{50} by 0.7 points over YOLOv12-M-P2 and exceeds the second-best $AP_{50:95}$ value of 19.5 achieved by YOLO11-M-P2 by 0.5 points.

In terms of efficiency, although CollabOD introduces slightly more parameters at 29.9M, it achieves the lowest computational cost of 65.5 GFLOPs and the highest inference speed of 137 FPS, demonstrating a superior accuracy–efficiency trade-off.

These results indicate that the proposed collaborative detection framework effectively enhances small-object detection performance on AI-TOD while maintaining competitive real-time capability.

2) *Ablation Studies:* On the AI-TOD dataset, we conduct an ablation study to evaluate the contribution of each component in the proposed framework, as shown in Table V. Starting from the baseline model, which achieves 44.5 AP_{50} and 19.5 $AP_{50:95}$ with 91.3 GFLOPs and 101 FPS, we

TABLE IV
COMPARISON ON THE AI-TOD [13] DATASET. THE BEST RESULTS AMONG YOLO-SERIES MODELS ARE HIGHLIGHTED IN BOLD.

Model	AP_{50}	$AP_{50:95}$	Params	GFLOPs	FPS
YOLOv8-M-P2 [48]	44.1	19.3	25.0	99.0	92
YOLOv10-M-P2 [49]	43.9	18.7	23.2	142.5	127
YOLO11-M-P2 [10]	44.5	19.5	20.7	91.3	101
YOLOv12-M-P2 [40]	44.7	17.2	20.0	94.4	107
CollabOD	45.4	20.0	29.9	65.5	137

TABLE V
ABLATION STUDY ON THE AI-TOD [13] DATASET. EACH COMPONENT OF THE PROPOSED FRAMEWORK IS INCREMENTALLY ADDED TO EVALUATE ITS INDIVIDUAL CONTRIBUTION. BOLD VALUES INDICATE THE BEST PERFORMANCE.

DPF-Stem	DABlock	BRM	UDA Head	Detection		Complexity	
				AP_{50}	$AP_{50:95}$	GFLOPs	FPS
				44.5	19.5	91.3	101
✓				43.2	18.4	51.2	110
✓	✓			43.7	18.8	68.2	107
✓	✓	✓		44.2	19.3	74.8	118
✓	✓	✓	✓	45.4	20.0	65.5	137

progressively incorporate DPF-Stem, DABlock, BRM, and the UDA Head.

Introducing DPF-Stem improves the inference speed to 110 FPS while reducing the computational cost to 51.2 GFLOPs, with a slight fluctuation in detection accuracy. Adding DABlock further enhances AP_{50} to 43.7 and $AP_{50:95}$ to 18.8, demonstrating its effectiveness in strengthening feature representation. When BRM is incorporated, the detection performance increases to 44.2 AP_{50} and 19.3 $AP_{50:95}$, while maintaining efficient computation at 74.8 GFLOPs.

Finally, integrating the UDA Head yields the full CollabOD model, achieving the best overall performance with 45.4 AP_{50} and 20.0 $AP_{50:95}$, while simultaneously reducing the computational cost to 65.5 GFLOPs and increasing the inference speed to 137 FPS. These results verify that each component contributes positively to detection accuracy and efficiency, and their combination leads to a consistent and complementary performance gain.

V. CONCLUSIONS

We present CollabOD, a lightweight framework for UAV small object detection that improves localization stability by enhancing structural cues and calibrating feature streams prior to fusion. Experiments on VisDrone, UAVDT, and AI-TOD demonstrate improved performance under stricter IoU thresholds with competitive efficiency. Future work will explore real-time onboard deployment and integration with downstream aerial tasks such as multi-object tracking and collaborative UAV perception.

ACKNOWLEDGMENT

This work is supported by Key Technologies for Automatic Inspection and Evaluation of Railway Infrastructure

REFERENCES

- [1] Z. Li, S. Lian, D. Pan, Y. Wang, and W. Liu, "Ad-det: Boosting object detection in uav images with focused small objects and balanced tail classes," *Remote Sensing*, vol. 17, no. 9, p. 1556, 2025.
- [2] M. Nikouei, B. Baroutian, S. Nabavi, F. Taraghi, A. Aghaei, A. Sajedi, and M. E. Moghaddam, "Small object detection: A comprehensive survey on challenges, techniques and real-world applications," *Intelligent Systems with Applications*, vol. 27, p. 200561, 2025. [Online]. Available: <https://www.sciencedirect.com/science/article/pii/S2667305325000870>
- [3] X. Zhao, H. Zhang, W. Zhang, J. Ma, C. Li, Y. Ding, and Z. Zhang, "Msud-yolo: A novel multiscale small object detection model for uav aerial images," *Drones*, vol. 9, no. 6, 2025. [Online]. Available: <https://www.mdpi.com/2504-446X/9/6/429>
- [4] J. Luo, K. Chang, J. Huang *et al.*, "A uav aerial image small object detection algorithm based on fine-grained feature preservation and multi-scale feature pyramid balancing," *Complex & Intelligent Systems*, vol. 12, p. 12, 2026. [Online]. Available: <https://doi.org/10.1007/s40747-025-02126-x>
- [5] Y. Xia, C. Liu, T. Xiang, and Z. Tu, "Efsi-detr: Efficient frequency-semantic integration for real-time small object detection in uav imagery," 2026. [Online]. Available: <https://arxiv.org/abs/2601.18597>
- [6] X. Wang, Y. Peng, and C. Shen, "Efficient feature fusion for uav object detection," 2025. [Online]. Available: <https://arxiv.org/abs/2501.17983>
- [7] L. Li, Z. Zhu, X. Zhao *et al.*, "MST-DETR: A multi-scale enhanced tiny object detection framework," *Signal, Image and Video Processing*, vol. 20, p. 5, 2026. [Online]. Available: <https://doi.org/10.1007/s11760-025-05074-8>
- [8] G. Ghiasi, T.-Y. Lin, and Q. V. Le, "Nas-fpn: Learning scalable feature pyramid architecture for object detection," in *Proceedings of the IEEE/CVF Conference on Computer Vision and Pattern Recognition*, 2019, pp. 7036–7045.
- [9] C. Guo, B. Fan, Q. Zhang, S. Xiang, and C. Pan, "Augfpn: Improving multi-scale feature learning for object detection," 2019. [Online]. Available: <https://arxiv.org/abs/1912.05384>
- [10] G. Jocher and J. Qiu, "Ultralytics yolo11," 2024. [Online]. Available: <https://github.com/ultralytics/ultralytics>
- [11] P. Zhu, L. Wen, D. Du, X. Bian, H. Fan, Q. Hu, and H. Ling, "Detection and tracking meet drones challenge," *IEEE Transactions on Pattern Analysis and Machine Intelligence*, pp. 1–1, 2021.
- [12] D. Du, Y. Qi, H. Yu, Y. Yang, K. Duan, G. Li, W. Zhang, Q. Huang, and Q. Tian, "The unmanned aerial vehicle benchmark: Object detection and tracking," in *Proceedings of the European Conference on Computer Vision (ECCV)*, 2018, pp. 370–386.
- [13] J. Wang, W. Yang, H. Guo, R. Zhang, and G.-S. Xia, "Tiny object detection in aerial images," in *Proceedings of the 25th International Conference on Pattern Recognition (ICPR)*. IEEE, 2021, pp. 3791–3798.
- [14] K. Liu, Z. Fu, S. Jin, Z. Chen, F. Zhou, R. Jiang, Y. Chen, and J. Ye, "Esod: Efficient small object detection on high-resolution images," *IEEE Transactions on Image Processing*, vol. 34, pp. 183–195, 2024.
- [15] F. C. Akyon, C. Cengiz, S. O. Altinuc, D. Cavusoglu, K. Sahin, and O. Eryuksel, "Sahi: A lightweight vision library for performing large scale object detection and instance segmentation," Nov. 2021. [Online]. Available: <https://doi.org/10.5281/zenodo.5718950>
- [16] J. Zhang, J. Lei, W. Xie, Z. Fang, Y. Li, and Q. Du, "Superyolo: Super resolution assisted object detection in multimodal remote sensing imagery," *IEEE Transactions on Geoscience and Remote Sensing*, vol. 61, pp. 1–15, 2023.
- [17] G. Yang, J. Lei, Z. Zhu, S. Cheng, Z. Feng, and R. Liang, "Afpn: Asymptotic feature pyramid network for object detection," *arXiv preprint arXiv:2306.15988*, 2023.
- [18] W. Lu, S.-B. Chen, H.-D. Li, Q.-L. Shu, C. H. Ding, J. Tang, and B. Luo, "Legnet: A lightweight edge-gaussian network for low-quality remote sensing image object detection," in *Proceedings of the IEEE/CVF International Conference on Computer Vision*, 2025, pp. 2844–2853.
- [19] Y. Wang, X. Bai, B. Hu, C. Xu, H. Chen, V. Chung, T. Li, and X. Chen, "Mgdfis: Multi-scale global-detail feature integration strategy for small object detection," *arXiv preprint arXiv:2506.12697*, 2025.
- [20] Y. Chen, X. Yuan, J. Wang, R. Wu, X. Li, Q. Hou, and M.-M. Cheng, "Yolo-ms: Rethinking multi-scale representation learning for real-time object detection," *IEEE Transactions on Pattern Analysis and Machine Intelligence*, vol. 47, no. 6, pp. 4240–4252, 2025.
- [21] T.-Y. Lin, P. Dollár, R. Girshick, K. He, B. Hariharan, and S. Belongie, "Feature pyramid networks for object detection," in *Proceedings of the IEEE/CVF Conference on Computer Vision and Pattern Recognition*, 2017, pp. 2117–2125.
- [22] K. Wang, J. H. Liew, Y. Zou, D. Zhou, and J. Feng, "Panet: Few-shot image semantic segmentation with prototype alignment," in *Proceedings of the IEEE/CVF International Conference on Computer Vision*, 2019, pp. 9197–9206.
- [23] S. Liu, L. Qi, H. Qin, J. Shi, and J. Jia, "Path aggregation network for instance segmentation," in *Proceedings of the IEEE/CVF Conference on Computer Vision and Pattern Recognition*, 2018, pp. 8759–8768.
- [24] S. Liu, D. Huang, and Y. Wang, "Learning spatial fusion for single-shot object detection," *arXiv preprint arXiv:1911.09516*, 2019.
- [25] Z. Yang, Q. Guan, Z. Yu, X. Xu, H. Long, S. Lian, H. Hu, and Y. Tang, "Mhaf-yolo: Multi-branch heterogeneous auxiliary fusion yolo for accurate object detection," *arXiv preprint arXiv:2502.04656*, 2025.
- [26] X. Lin, J. Peng, Z. Gan, J. Zhu, and J. Liu, "Yolo-master: Moe-accelerated with specialized transformers for enhanced real-time detection," *arXiv preprint arXiv:2512.23273*, 2025.
- [27] J. Zhang, M. Chen, Y. Zhao, L. Shan, C. Li, H. Hu, X. Ge, Q. Zhu, and B. Xu, "Asymmetric mamba-cnn collaborative architecture for large-size remote sensing image semantic segmentation," *IEEE Transactions on Geoscience and Remote Sensing*, vol. 63, pp. 1–19, 2025.
- [28] Z. Yang, Z. Li, X. Jiang, Y. Gong, Z. Yuan, D. Zhao, and C. Yuan, "Focal and global knowledge distillation for detectors," in *Proceedings of the IEEE/CVF Conference on Computer Vision and Pattern Recognition*, 2022, pp. 4643–4652.
- [29] J. Zhuang, Z. Qin, H. Yu, and X. Chen, "Task-specific context decoupling for object detection," *arXiv preprint arXiv:2303.01047*, 2023.
- [30] H. Rezatofghi, N. Tsoi, J. Gwak, A. Sadeghian, I. Reid, and S. Savarese, "Generalized intersection over union: A metric and a loss for bounding box regression," in *Proceedings of the IEEE/CVF Conference on Computer Vision and Pattern Recognition*, 2019, pp. 658–666.
- [31] Y.-F. Zhang, W. Ren, Z. Zhang, Z. Jia, L. Wang, and T. Tan, "Focal and efficient iou loss for accurate bounding box regression," *Neurocomputing*, vol. 506, pp. 146–157, 2022.
- [32] Z. Zheng, P. Wang, W. Liu, J. Li, R. Ye, and D. Ren, "Distance-iou loss: Faster and better learning for bounding box regression," in *Proceedings of the AAAI Conference on Artificial Intelligence*, vol. 34, no. 07, 2020, pp. 12 993–13 000.
- [33] S. Xu, X. Wang, W. Lv, Q. Chang, C. Cui, K. Deng, G. Wang, Q. Dang, S. Wei, Y. Du, and B. Lai, "Pp-yoloe: An evolved version of yolo," *arXiv preprint arXiv:2203.16250*, 2022.
- [34] Z. Du, Z. Hu, G. Zhao, Y. Jin, and H. Ma, "Cross-layer feature pyramid transformer for small object detection in aerial images," *IEEE Transactions on Geoscience and Remote Sensing*, 2025.
- [35] C. Yang, Z. Huang, and N. Wang, "Querydet: Cascaded sparse query for accelerating high-resolution small object detection," in *Proceedings of the IEEE/CVF Conference on Computer Vision and Pattern Recognition*, 2022, pp. 13 668–13 677.
- [36] K. Wang, X. Fu, Y. Huang, C. Cao, G. Shi, and Z.-J. Zha, "Generalized uav object detection via frequency domain disentanglement," in *Proceedings of the IEEE/CVF Conference on Computer Vision and Pattern Recognition*, 2023, pp. 1064–1073.
- [37] H. Zhang, H. Zhang, K. Liu, Z. Gan, and G.-N. Zhu, "Uav-detr: efficient end-to-end object detection for unmanned aerial vehicle imagery," in *2025 IEEE/RSJ International Conference on Intelligent Robots and Systems (IROS)*. IEEE, 2025, pp. 15 143–15 149.
- [38] S. Huang, C. Lin, X. Jiang, and Z. Qu, "Brstd: Bio-inspired remote sensing tiny object detection," *IEEE Transactions on Geoscience and Remote Sensing*, vol. 62, pp. 1–15, 2024.
- [39] L. Wei, S. Sun, J. Yao, Y. Mi, X. Sui, H. Chen, and S. Liu, "Uav-malo: Mamba-augmented yolo hybrid architecture for uav micro-object detection in autonomous robotics," in *2025 IEEE/RSJ International Conference on Intelligent Robots and Systems (IROS)*. IEEE, 2025, pp. 8187–8193.
- [40] Y. Tian, Q. Ye, and D. Doermann, "Yolo12: Attention-centric real-time object detectors," *arXiv preprint arXiv:2502.12524*, 2025.
- [41] G. Jocher and J. Qiu, "Ultralytics yolo26," 2026. [Online]. Available: <https://github.com/ultralytics/ultralytics>
- [42] T.-Y. Lin, M. Maire, S. Belongie, J. Hays, P. Perona, D. Ramanan, P. Dollár, and C. L. Zitnick, "Microsoft coco: Common objects in context," in *Proceedings of the European Conference on Computer Vision (ECCV)*. Springer, 2014, pp. 740–755.

- [43] F. Yang, H. Fan, P. Chu, E. Blasch, and H. Ling, "Clustered object detection in aerial images," in *The IEEE International Conference on Computer Vision (ICCV)*, October 2019.
- [44] S. Deng, S. Li, K. Xie, W. Song, X. Liao, A. Hao, and H. Qin, "A global-local self-adaptive network for drone-view object detection," *IEEE Transactions on Image Processing*, vol. 30, pp. 1556–1569, 2021.
- [45] J. Zhang, J. Huang, X. Chen, and D. Zhang, "How to fully exploit the abilities of aerial image detectors," in *Proceedings of the IEEE/CVF International Conference on Computer Vision Workshops*, 2019.
- [46] X. Li, W. Wang, L. Wu, S. Chen, X. Hu, J. Li, J. Tang, and J. Yang, "Generalized focal loss: Learning qualified and distributed bounding boxes for dense object detection," in *Advances in Neural Information Processing Systems (NeurIPS)*, 2020.
- [47] B. Du, Y. Huang, J. Chen, and D. Huang, "Adaptive sparse convolutional networks with global context enhancement for faster object detection on drone images," in *Proceedings of the IEEE/CVF Conference on Computer Vision and Pattern Recognition*, 2023, pp. 13 435–13 444.
- [48] G. Jocher, A. Chaurasia, and J. Qiu, "Ultralytics yolov8," 2023. [Online]. Available: <https://github.com/ultralytics/ultralytics>
- [49] A. Wang, H. Chen, L. Liu *et al.*, "Yolov10: Real-time end-to-end object detection," *arXiv preprint arXiv:2405.14458*, 2024.